ANALYSIS OF ANISOTROPIC CONDUCTORS ON ANISOTROPIC SUBSTRATES

Mohamed A. Megahed, and Samir M. El-Ghazaly

Department of Electrical Engineering
Telecommunications Research Center
Arizona State University
Tempe, Arizona 85287-5706

ABSTRACT

A full-wave finite-difference time-domain technique is used to study the anisotropy associated with anistropic conductors on anisotropic substrates. The scheme is applied to analyze high temperature superconductor (HTS) YBCO film deposited on anisotropic sapphire substrate. The effect of the anisotropy on the performance of the coplanar wave guide and the microstrip line is evaluated. The losses and the dispersion characteristics, as well as the current distributions inside the HTS, are calculated. It is shown that the 90^{o} r-cut sapphire substrate structure has lower loss and lower effective dielectric constant than the 0^{o} r-cut substrate.

INTRODUCTION

In this paper, the anisotropy of the conductors and the substrates, used in many microwave and millimeter-wave devices, are simultaneously taken into account using a full-wave finite-difference time-domain analysis. The anisotropy associated with both the HTS materials, as $YBa_2Cu_3O_X$, and TlBaCaCuO, and the substrates, such r-cut single crystal sapphire is analysed, as a case study. This anisotropy affects the performance of HTS microwave and millimeter-wave devices. The physical characteristics of the HTS are blended with the electromagnetic model using the phenomenological two fluid model. The effects of the anisotropy on the field distribution inside the structure, as well as currents distribution inside the HTS, are studied. The developed model is applied to investigate anisotropic microstrip lines and anisotropic coplanarwave guides. Interesting comparisons between isotropic and anisotropic structures as well as comparison between the characteristics of the microstrip lines versus coplanar waveguides will be presented.

ANISOTROPIC SUPERCONDUCTOR MODEL

The two fluid model assumes that the electron gas in a superconductor material consists of two gases, the superconducting electron gas and the normal electron gas [1]. The main parameters of the superconducting material are the London penetration depth λ_L and the normal conductivity σ_n. The total current density in superconducting material is expressed as follows

$$\mathbf{J} = \mathbf{J}_n + \mathbf{J}_s , \qquad (1)$$

where J_n and J_s are the normal state and super state current densities, respectively. The normal fluid current density obeys Ohm's law

$$\mathbf{J}_n = \sigma_n \mathbf{E} . \qquad (2)$$

The superconducting fluid current density is obtained using London equation [1],

$$\frac{\partial \mathbf{J}_s}{\partial t} = \frac{1}{\mu_o \lambda_L^2} \mathbf{E} . \qquad (3)$$

These expressions are valid assuming that the HTS material is isotropic. However, experiments show that the properties of the HTS materials are anisotropic. Such anisotropy may have significant effects on the device performance. The designer is faced with several choices, as the type of materials, film direction, to obtain the optimum configuration that enhances the characteristics of the HTS material. The anisotropy for the HTS can be represented by an anisotropic conductivity for the normal state, and an anisotropic London penetration depth for the superconducting state. The diagonal conductivity tensor $\bar{\sigma}$ is given by

$$\bar{\sigma} = \begin{bmatrix} \sigma_a & 0 & 0 \\ 0 & \sigma_b & 0 \\ 0 & 0 & \sigma_c \end{bmatrix} . \qquad (4)$$

Also, the diagonal London penetration depth tensor $\bar{\lambda}$ is described as follows,

CH3577-4/95/0000-0353$01.00 © 1995 IEEE

$$\underline{\lambda} = \begin{bmatrix} \lambda_a & 0 & 0 \\ 0 & \lambda_b & 0 \\ 0 & 0 & \lambda_c \end{bmatrix}, \quad (5)$$

where a, b and c are the principal axes of the anisotropic superconducting material. The normal conductivity and the London penetration depth in equations (1)-(3) will be replaced by their corresponding tensors to formulate the anisotropic superconductor model.

Experiments show that, for YBCO, the HTS parameters along the a- and b-axes are approximately equal. The normal conductivity σ_{nab} equals 10-80 times σ_{nc}, and the penetration depth λ_c equals 3-5 times λ_{ab} [2]. Experiments also report that the critical current density and the upper critical field are anisotropic.

ANISOTROPIC FINITE-DIFFERENCE TIME-DOMAIN APPROACH

An arbitrary 3-D structure can be embedded in a FDTD lattice simply by assigning desired values of the material parameters (e.g. electrical permittivity, conductivity, and London penetration depth) to each lattice point. These parameters are utilized in the calculation of the respective electromagnetic field components. The material parameters are interpreted by the FDTD program as *local coefficients* for the time-stepping algorithm [3]. Specification of the media properties in this component-by-component manner provides a convenient algorithm to represent the anisotropy in a media, and assures continuity of tangential fields at the interface of dissimilar media with no need for special field matching. The developed three-dimensional finite-difference time-domain scheme is capable of modeling the finite thickness of the HTS strip. The finite thickness is represented by adequate number of mesh points. A graded non uniform mesh generator is used to dicsretize the simulation domain [4]. The ground plane is chosen as a perfect electric wall, for simplicity. The computational domain is closed by the PML absorbing boundary conditions. The program code for our analysis is written in FORTRAN 90 and is executed in massively parallel machine (MASPAR) environment. The anisotropy is included in the FDTD code without significantly affecting its efficiency or the required memory size.

In our discussion, the YBCO HTS strip is assumed to be anisotropic along its principal axis (*i.e.* c, b, and a along x, y, and z respectively), as shown in Fig. 1. The r-cut sapphire substrate is considered for two cases at 0 and 90 degrees rotation about its principal axis (*i.e.* rotation about x-axis). The configuration simulated in this study corresponds to the practical structure used in [5]. However, the analysis presented here is flexible and can be extended to any anisotropic configuration. The same algorithm can be implemented when the principal axes of the anisotropic material are tilted with respect to the coordinates. In this case, the solution will be carried on the electric (**D**) and magnetic (**B**) flux densities. The algorithm will be extended one step further, to obtain the field intensity using the appropriate constitutive relations.

RESULTS AND DISCUSSIONS

A microstrip line and coplanar waveguide with YBCO HTS material on sapphire substrates are analyzed using the previously described technique. The frequency independent penetration depth and the normal conductivity of the HTS equal to 0.2 μm and 1.0×10^6 S/m, respectively at 77K for both structures. The dimensions of the microstripline are as follows : strip width 2W = 2 μm, substrate height h = 1 μm, and HTS strip thickness t = 0.5 μm. The coplanar waveguide has the same dimensions with slot width of s = 0.5 μm. These dimensions are selected to allow comparing our results with those presented in [6] and [7]. The anisotropic characteristics of the HTS are presented by anisotropic penetration depth, $\lambda_c = 5\ \lambda_{ab}$, and anisotropic normal conductivity, $\sigma_{nab} = 50\ \sigma_{nc}$ for both structures [2]. The principal axes of the HTS film is aligned with the coordinate axes. The c-axis is assumed to be in the x-direction. The anisotropy of the sapphire substrate is represented by the dielectric permittivity tensor. For the 0^o r-cut sapphire, the relative permittivity tensor is $\varepsilon_{xx} = 10.03$, $\varepsilon_{yy} = 10.97$, and $\varepsilon_{zz} = 9.4$ along x, y, and z directions respectively. The tensor is $\varepsilon_{xx} = 10.03$, $\varepsilon_{yy} = 9.4$ and $\varepsilon_{zz} = 10.97$ for the 90^o r-cut [5]. The angle is calculated with respect to the rotation about the x-axis. To assess the effect of the substrate anisotropy, a comparison will be made between the performance of both transmission lines on sapphire substrates with similar structures on isotropic substrates with a relative permittivity $\varepsilon_r = 10.03$.

The microstrip line dimensions are presented in Fig. 2. Fig. 3 shows the attenuation constant for the anistropic HTS on r-cut sapphire substrate as a function of the rotation angle about the x-axis at two different angles, 0^o and 90^o and for anistropic HTS on isotropic substrate with $\varepsilon_r = 10.03$. The microstrip line on anisotropic sapphire substrate with 0^o r-cut has the highest attenuation. The 90^o r-cut produces the lowest attenuation of the three structures. The effective dielectric constants ε_{reff} of the three structures are also depicted in Fig. 3. The 0^o r-cut sapphire substrate results in the highest ε_{reff}, while the 90^o r-cut substrate produces the lowest. The change in the propagation characteristics can be explained by the value of the permittivity tensor element ε_{yy} in the y-direction. The y-field component of the fringing field increases with the increase of ε_{yy} from 9.4 (90^o rotation) to 10.03 (isotropic) to 10.97 (0^o rotation) which in turn increases the energy stored in the substrate, and results in the

decrease of the propagating wave velocity on the line or increase in the effective dielectric constant. The increase in the attenuation constant can be explained by considering the various current distributions presented in Fig. 4. It is shown that the normal current density is the largest for the 0^o r-cut and it is the lowest for the 90^o r-cut substrate. This explains the slightly higher attenuation in the 0^o r-cut case.

The coplanar waveguide dimensions are demonstrated in Fig. 5. The effective dielectric constant and attenuation constant, and the current densities distribution are calculated as the microstrip line case and shown in Fig. 6 and Fig. 7, respectively. The coplanar waveguide on anisotropic sapphire substrate with 0^o cut has the highest attenuation and highest effective dielectic constant, while the 90^o r-cut substrate results in the lowest ones. The change in the propagation characteristics can be explained by the value of the permittivity tensor element ε_{yy} in the y-direction. It is known that the electric field in the y-direction is the strongest field component in the coplanar waveguide. This results in an increase in the energy stored in the substrate as the permittivity tensor element ε_{yy} increases, which in turn decreases the phase velocity of the propagating wave along the transmission line. The increase in the attenuation constant can be justified by considering the various current distributions presented in Fig. 7. It is observed that the normal current density is the largest for the 0^o r-cut and it it is the lowest for the 90^o r-cut sapphire substrate. This explains the slightly higher attenuation in the 0^o r-cut case.

Comparison of the anisotropy effects on both the microstrip line and the coplanar waveguide can be depicted by analyzing Fig. 3 and Fig. 6. One should observe that the change in the propagation characteristics for the presented coplanar waveguide with the anisotropy of the materials is more pronounced than the microstrip line.

CONCLUSION

A full-wave analysis for anisotropic HTS planar microwave structures deposited on anisotropic substrates, is presented. The FDTD technique, which takes the finite thickness of the anisotropic HTS film into consideration, is developed using a graded non uniform mesh generator. The propagation characteristics of the anisotropic HTS microstrip line and coplanar wave guide, on r-cut sapphire substrate, are calculated as functions of different r-cut angles. It is shown that the 90^o r-cut sapphire substrate structure has lower loss and lower effective dielectric constant than the 0^o r-cut one for both structures. These observations are explained by the current distributions on the HTS strip. The approach presented can be used not only to obtain the characteristics of HTS microwave structures but also to determine the optimum design that exploits the anisotopic conductor characteristics on anisotropic substrates.

ACKNOWLEDGMENT

This work was supported by the National science foundation under Grant ECS-9108933.

REFERENCES

[1] T. Van Duzer and C. W. Turner, *Principles of Superconductive Devices and Circuits.* New York: Elsevier, 1981.

[2] Y. Iye, "Studies of High Temperature Superconductors : *Anisotropic Superconducting and Normal State Transport Properties of HTSC Single Crystals*," New York: Nova, 1989.

[3] K. S. Yee, "Numerical Solution of initial boundary problems involving Maxwell's equations in isotropic media," *IEEE Trans. Antennas Propagation*, vol. 14, pp. 302-307, 1966.

[4] M. A. Megahed, S. A. El-Ghazaly, "Finite difference approach for rigorous full-wave analysis of superconducting microwave structures," *IEEE MTT-S Int. Microwave Symp. Dig.*, June 1993.

[5] I. B. Vendik et al., "CAD Model for Microstrips on r-cut Sapphire Substrates," submitted to *Int. Joun. of Microwave and Millimeter-Wave Computer-Aided Engineering*, 1994.

[6] L. Lee, S. Ali, and W. Lyons, "Full-Wave Characterization of High-Tc Superconducting Transmission Lines," *IEEE Trans. Appl. Superconduct.*, vol. 2, no. 9, pp. 49-57, 1992.

[7] M. A. Megahed, S. A. El-Ghazaly, "Analysis of Anisotropic High Temperature Superconductor Planar Structures on Sapphire Anisotropic Substrates," submitted to *IEEE Trans. Microwave Theory Tech., 1994.*.

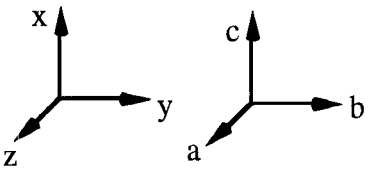

Fig. 1 Principal axes of HTS and coordinate axes

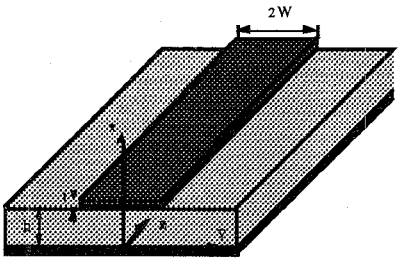

Fig. 2 Anisotropic HTS microstrip line on anisotropic substrate

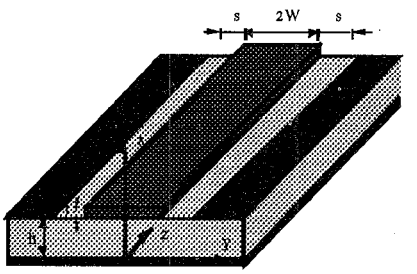

Fig. 5 Anisotropic HTS coplanar waveguide on anisotopic substrate

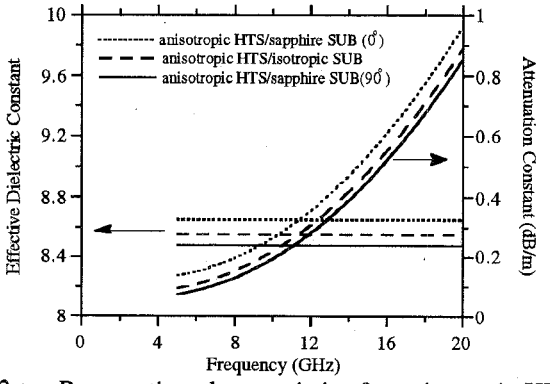

Fig. 3 Propagation characteristics for anisotropic HTS on different r-cut anisotropic sapphire substrates.

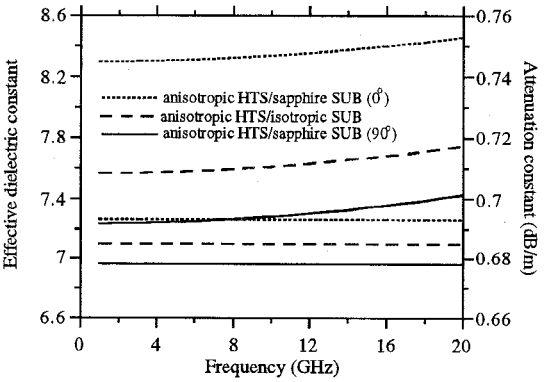

Fig. 6 Propagation characteristics for anisotropic HTS on different r-cut anisotropic sapphire substrates.

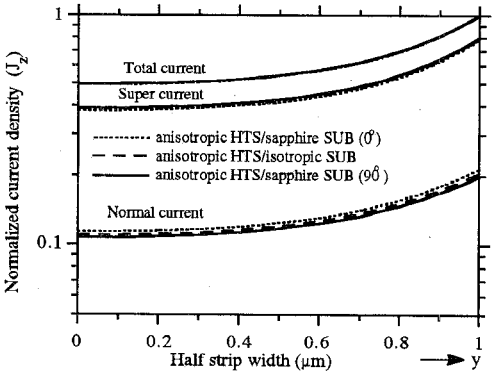

Fig. 4 Normal-fluid, superconducting-fluid, and total current densities for anisotropic HTS on different r-cut sapphire substrates.

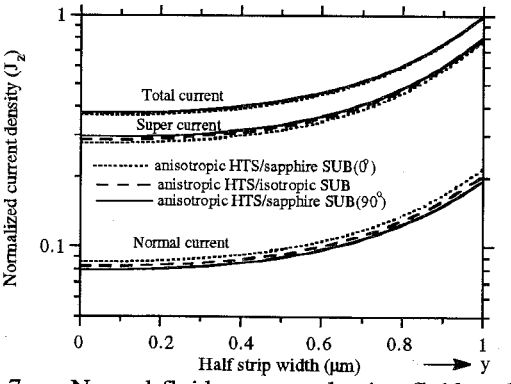

Fig. 7 Normal-fluid, superconducting-fluid, and total current densities for anisotropic HTS on different r-cut sapphire substrates.